Journal of Alloys and Compounds 899 (2022) 163323

Contents lists available at ScienceDirect

Journal of Alloys and Compounds

journal homepage: www.elsevier.com/locate/jalcom

Influence of deep cryogenic treatment on natural and artificial aging of Al-Mg-Si alloy EN AW 6026

Matic Jovičević-Klug[a,b], Rok Rezar[b], Patricia Jovičević-Klug[b,c,*], Bojan Podgornik[b,c]

[a] Max-Planck-Institut für Eisenforschung, Max-Planck-Strasse 1, 40237 Düsseldorf, Germany
[b] Department of Metallic Materials and Technology, Institute of Metals and Technology, Lepi pot 11, 1000 Ljubljana, Slovenia
[c] Jožef Stefan International Postgraduate School, Jamova cesta 39, 1000 Ljubljana, Slovenia

ARTICLE INFO

Article history:
Received 14 October 2021
Received in revised form 30 November 2021
Accepted 16 December 2021
Available online 20 December 2021

Keywords:
Aluminum alloy
Microstructure
Mechanical properties
Precipitation
Dispersoids
Deep cryogenic treatment

ABSTRACT

This paper discusses the effect of deep cryogenic treatment (DCT) on the evolution of natural and artificial aging of Al-Mg-Si alloy EN AW 6026. This study provides the first research and evidence of DCT effect on dispersoids and their development in aluminum alloys. DCT induces reformation and regrowth of dispersoids during natural aging from a preferential cuboidal shape to spherical, which is also distinguishable by the change in chemical composition. Additionally, with DCT the dispersoids form in a denser manner, which consequently influences the hardness evolution with aging time. The study also reveals that the exposure duration to DCT (from 24 to 48 h) increases the DCT impact on the hardness evolution during natural aging of selected alloy. The influence of homogenization temperature on the DCT performance is also researched in connection to modified natural aging, which is correlated to the presence and formation of secondary phases during homogenization. Furthermore, DCT also promotes the formation of β'' precipitates and at the same time retards the formation of larger β' precipitates during artificial aging. After artificial aging, both dispersoids and precipitates display a denser population and more elongated shape aligned along the < 100 > axis of the aluminum matrix with DCT compared to conventionally heat-treated samples without DCT. The microstructural changes during DCT application are strongly linked to the modification of dispersoids with homogenization and artificial aging that influence the content of alloying elements in the matrix.

1. Introduction

Al-Mg-Si alloys, also denoted as series 6xxx aluminum alloys, are formable alloys that have very good corrosion resistance and anodizing properties with relatively good mechanical properties. Furthermore, these alloys are easily extruded, welded and machined and are also heat-treatable, allowing improvement of mechanical properties by aging after material forming. As a result, the 6xxx alloys are one of the most commonly used aluminum alloys in automotive, electrical, aerospace, shipbuilding and off-shore plant industries [1–3]. However, the research on processing of such alloys is still underway, leading to novel processes that allow improving properties of 6xxx alloys [4–7]. The potential of one such process, namely sub-zero heat treatment, deep cryogenic treatment (DCT), has been successfully tested on various ferrous alloys [8–10], while for non-ferrous alloys, such as the aforementioned aluminum alloys, DCT is still at its beginnings. As a result, there is still a great potential for the development and new findings of the mechanisms behind the changes in aluminum alloys induced by DCT. Nonetheless, the increase of the research in this field is expected to increase, due to the higher market demands of the development and improvement of specific aluminum alloys for development of light-weight vehicles in automotive industry and maritime industry [11]. Due to the lack of studies, only few studies have provided limited insight into the changes and mechanisms of DCT on aluminum alloys. Studies of cryogenic treatment have been performed on 2xxx [12,13], 5xxx [1,14], 6xxx [1,15–17] and 7xxx [18–21] series aluminum alloys. For 2xxx alloys DCT is confirmed to not have a role on strain hardening behavior [22]. Furthermore, Lee et al., 2004 [23] and Park et al., 2015 [1] observed an increase in tensile and yield stress, hardening effect, fracture strain and ductility for 5xxx aluminum alloy after DCT application. Studies of 7xxx series aluminum alloys determined an increase in tensile strength [18], tensile yield strength [18], elongation [18], hardness [19], toughness [19], reduction of residual stress

* Corresponding author at: Department of Metallic Materials and Technology, Institute of Metals and Technology, Lepi pot 11, 1000 Ljubljana, Slovenia.
E-mail address: patricia.jovicevicklug@imt.si (P. Jovičević-Klug).

https://doi.org/10.1016/j.jallcom.2021.163323
0925-8388/

[20] and improvement in dimensional stability [20]. However, the study by Weng et al., 2021 [21] observed contrary results after application of DCT. Some studies [1,15,17] reported improved properties such as wear resistance, hardness and tensile strength of 6xxx after DCT. These studies suggest that the size and number of precipitates and decreased solubility of the alloying elements could be responsible for the modified characteristics of alloy with DCT, which originates from the altered natural aging of the 6xxx alloys.

As mentioned, the 6xxx aluminum alloys can be further hardened and strengthened with appropriate heat treatment. For this reason, the two-stage heat treatment is used, consisting of homogenization and ageing process. In the first step, homogenization is applied to redistribute the alloying elements within the α-Al phase and to change the Al, Mg, Si-based precipitation within the alloys. This process is usually performed in the temperature range between 450 °C and 600 °C for 6xxx aluminum alloys [24]. The exact selection of the homogenization temperature depends on the alloying content and ratio between Mg and Si of the alloy [25,26] as well as on the presence of other alloying elements, such as Cu, Cr, Fe, Mn [27]. The second step, ageing, can be either natural (at room temperatures) or artificial (elevated temperatures). Ageing is performed in order to induce precipitation of various phases from the supersaturated solid solution (SSS), formed after quenching, and to increase precipitation strengthening of the aluminum alloy [28]. During natural ageing of 6xxx aluminum alloys, precipitation of clusters and Guinier-Preston (GP)-zones occurs, which results in a temporal hardness increase (denoted also as age-hardening) [27,29]. In contrast, artificial ageing of 6xxx aluminum alloy results in an increase of hardness and tensile strength and decrease in plasticity. The altered mechanical properties are a consequence of the growth of additional transiting metastable precipitates that are larger than the GP-zones, leading to higher strengthening phenomenon [30]. In artificial ageing the temperature and duration of artificial ageing can be manipulated, in order to obtain preferable size, type and quantity of precipitated phases [31], which influence the hardening process and with it also the development of corrosion, wear and mechanical properties [24]. The precipitation of phases follows Eq. 1 as described by Vissers et al., 2007 [25]:

$$SSS \rightarrow GP \rightarrow precipitates$$

$$\beta''((Al+Mg)_5Si_6) \rightarrow \beta''(Mg_5Si_6, \quad Al_3MgSi_6)$$

$$\rightarrow \beta'(Mg_9Si_5) + \beta' + U_1(MgAl_2Si_2,\ MgAl_4Si_5) + U_2(Mg_2Al_4Si_5,\ MgAlSi) \rightarrow \beta(Mg_2Si) \quad (1)$$

The metastable phases β', U_1 and U_2 coexist during β'-phase transition. The increased hardness is mainly related to the development of β' phases during the aging process, at which the hardening process decays with further progressing formation towards the stable β phase [32]. The precipitation is also determined by the alloying composition [26], which improves the hardness and strength of the alloy with increasing Mg:Si ratio [25].

The combined effect of DCT and aging of 6xxx alloys is scarcely researched in terms of modification of the aging process with DCT, with only one study [16] directly determining that DCT accelerates the precipitation of β'' precipitates during natural aging. However, the same authors show that the accelerated precipitation did not lead to increased hardness after natural aging and that improved hardness occurs with DCT only when additional paint bake treatment is performed.

Another aspect of 6xxx alloys is the presence of dispersoids that are formed from complex intermetallic structures consisting of heavier alloying elements such as Cr, Mn, Zr and Fe together with Al, Si and Mg [33]. The dispersoids have been predominantly used to refine the grain structure of the alloys [27,34]. However, with the rise of interest of these alloys for automotive industry, the research on dispersoids and their effect on the microstructure and its evolution with different heat treatments is on the rise [27]. As a result, many researchers have found that dispersoids can significantly modify the microstructure and the aging properties of the Al-Mg-Si alloys that depend on the dispersoid type, presence and amount of heavier alloying elements and the dispersoid density [27,33–39]. To the authors knowledge, no research has been performed so far on the DCT effect on dispersoid formation and their evolution during aging.

From the above, it can be concluded that there is a lack of research and understanding of the DCT influence on aging behavior of 6xxx series aluminum alloys. As a result, the EN AW 6026, selected as a representative alloy of the 6xxx aluminum series, which holds a variety of different alloying elements (Bi, Cu, Cr, Fe, Mg, Mn, Si and Pb), was subjected to DCT and was naturally and artificially aged. The aim of the study is to provide deeper insight into DCT induced microstructural changes for both natural and artificial aging states and correlate them to changes of selected mechanical properties. Furthermore, the study also considers different homogenization temperatures in order to understand the influence of homogenization temperature on the DCT modification of aging process of 6xxx alloys. Finally, the goal of this study is also to provide explanations and possible mechanisms behind DCT effect on the aging processes of 6xxx aluminum alloys from a microstructural standpoint.

2. Materials and methods

2.1. Material and heat treatment

For this research commercially available EN AW 6026 alloy rods, provided by Impol, Slovenia, were machined into different test samples for the different mechanical tests. The exact chemical composition of the investigated alloy, determined with inductively coupled plasma-optical emission spectrometry (ICP-OES) with Agilent 720, is provided in Table 1. The samples were cleaned and prepared for the different heat treatment procedures, which are schematically presented in Fig. 1(a). Firstly, the samples were separated into two major groups which were firstly homogenized in a standard muffle furnace for 1 h at different temperatures. The first group at 530 °C and the second at 570 °C. The exact temperature profiles of the homogenization are provided in Fig. 1(b). After homogenization the samples were quenched in water with an average temperature of 22 °C. After quenching the samples were dried and sorted into subsets for further processing. Half of the samples, denoted as deep cryogenic heat-treated (DCT), of both major groups were immersed in liquid nitrogen for 24 h or 48 h and afterwards warmed up to room temperature in ambient environment and finally aged. The other half of the samples, denoted as conventionally heat-treated (CHT), was directly aged after quenching. The aging for both CHT and DCT samples was performed at room temperature (natural aging) and at temperature of 190 °C (artificial aging) on separate sample subgroups. The natural aging was performed in a dry storage in ambient environment up to 28 days, whereas the artificial aging was performed for 8 h in a convection furnace. The time and temperature parameters of all heat

Table 1
Chemical composition of researched EN AW 6026.

Element	%Mg	%Si	%Bi	%Mn	%Pb	%Cu	%Fe	%Cr	%Ti	%Zn	%Sn	Al
Measured	0.70	0.68	0.66	0.59	0.34	0.30	0.27	0.045	0.029	0.025	< 0.005	balance

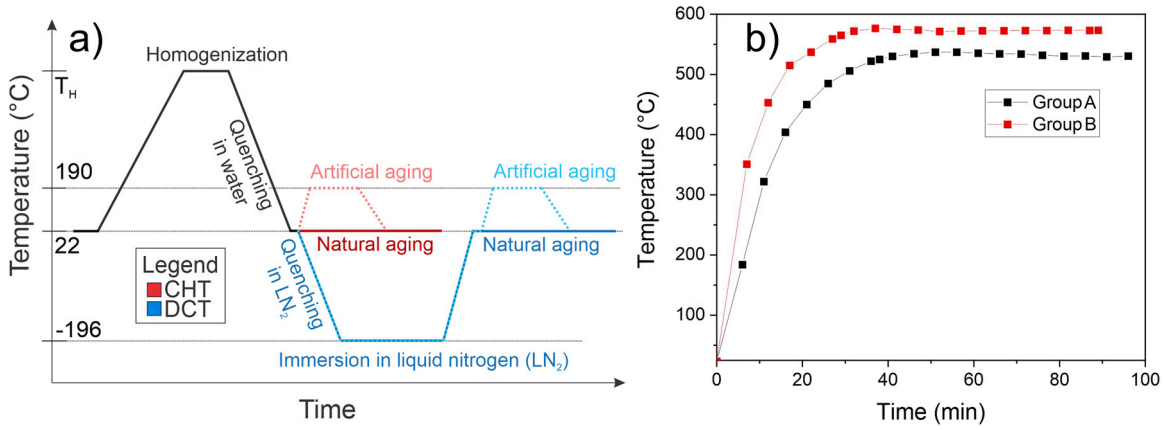

Fig. 1. a) Scheme of the heat treatment procedure for conventionally heat-treated (CHT) and cryogenic heat-treated samples encompassing homogenization at selected homogenization temperature (T_H), quenching in water, natural aging (dark color scheme) and artificial aging (light color scheme) with and without immersion in liquid nitrogen (LN_2). b) Temperature profiles of the major sample groups during homogenization.

Table 2
Time (t) and temperature (T) of individual heat treatment steps for sample groups that were naturally aged with and without deep cryogenic treatment (DCT).

Samples		Homogenization		DCT		Natural aging	
		T (°C)	t (h)	T (°C)	t (h)	T (°C)	t (days)
Group A	w/o DCT	530	1	/	/	22	1, 6, 14, 21, 28
	DCT 24 h	530	1	-196	24		
	DCT 48 h	530	1	-196	48		
Group B	w/o DCT	570	1	/	/		
	DCT 24 h	570	1	-196	24		
	DCT 48 h	570	1	-196	48		

Table 3
Time (t) and temperature (T) of individual heat treatment steps for sample groups that were artificially aged with and without deep cryogenic treatment (DCT).

Sample groups	Homogenization		DCT		Artificial aging	
	T (°C)	t (h)	T (°C)	t (h)	T (°C)	t (h)
1	530	1	/	/	190	8
2	530	1	-196	48		
3	570	1	/	/		
4	570	1	-196	48		

treatment procedures for both CHT and DCT samples with natural and artificial aging is provided in Table 2 and Table 3, respectively. The temperatures and time parameters were selected based on calculated data extracted from JMatPro, which are available in, to induce varying homogenized states and precipitation within a selected time frame for the individual processing steps. After different elapsed times of natural aging, the microstructure and hardness were evaluated to monitor the natural aging process. For the artificially aged samples, the mechanical properties and microstructure were measured after completion of the aging process.

2.2. Mechanical testing

2.2.1. Brinell hardness measurement

The Brinell method (SIST EN ISO 6506–1:2014 standard; HBW 2.5/62.5) was used to measure hardness, performed on the Charpy V-notched (CVN) samples using Innovatest Nexus 7500 device. At least three measurements were made on each sample. Before the measurements, the samples were properly prepared by grinding and polishing. For the naturally aged samples, the hardness was measured after 1 day, 6 days, 14 days, 21 days and 28 days after the homogenization (w/o DCT group) or DCT treatment (24 h DCT and 48 h DCT group). For the artificially aged samples, the hardness was measured after the complete heat treatment.

2.2.2. Tensile test

Tensile tests were performed using universal testing machine Instron 8802 with an Instron extensometer with initial gage length of 50 mm. The samples were manufactured according to the DIN 50125:2016 standard, type B with a diameter of 10 mm and a gauge length of 50 mm. Tensile tests were performed according to SIST EN ISO 6892–1:2017 standard using the A224 method. The initial strain rate was 0.00025 s^{-1} and after determining the yield strength, the rate was increased to 0.0067 s^{-1}. The recorded data are the average results obtained from the measurements of three specimens.

2.2.3. Impact toughness

Impact toughness was measured with the Charpy impact test at room temperature according to international standard SIST EN ISO 148–1:2017 using CVN specimens and 300 J pendulum.

2.2.4. Fatigue

Fatigue behavior of the investigated EN AW 6026 alloy was tested under dynamic loading in bending mode using Rumul resonant fatigue testing machine Cracktronic with an operating frequency of around 180 Hz. The fatigue (S/N) curves were obtained by performing room temperature fatigue tests on standard Charpy V-notched (CVN) samples (10 ×10×55 mm) and using constant amplitude bending stress between 70 MPa and 120 MPa, stress ratio R of 0.1 and a sinusoidal waveform. Sample failure criterion was set as a drop of inherent oscillation by more than 3%, where the fatigue cracks occurred down to a depth of 3 mm.

2.3. Chemical and metallographic analysis

For metallographic analysis, the samples were subsequently cut, polished and their surface finished with colloidal silica (25–40 nm particle size, 15 N load, 3 min polishing time). The optimal sample preparation was selected based on previous research on this alloy [40]. The microstructural observations were carried out with scanning electron microscopy (Jeol JSM-6500 F and ZEISS Crossbeam 550) and light microscopy (Zeiss Axio Imager.Z2m) immediately after metallographic polishing and 24 h, 7 days, 14 days and 21 days after sample preparation. The samples were stored between the measurements in a dry storage space at room temperature. For statistical relevance, 6 samples were monitored with the same measurement scheme described above. The scanning electron microscopy was conducted with acceleration voltage of 15 kV and

working distance of 10 mm. The angled imaging with SEM was performed with an observation angle of 70 ° with a working distance of 19 mm. Chemical composition was analyzed by energy-dispersive X-ray spectroscopy (Oxford EDS INCA Energy 450, detector type INCA X-SIGHT LN2).

For transmission electron microscopy (TEM) and scanning TEM (STEM), samples were prepared from 3 mm wide, 1 mm high and 1 mm thick lamellas, which were thinned by grinding and polishing using SiC papers to around 100–150 µm thickness and additionally ion-milled using JEOL EM-09100IS Ion Slicer (JEOL, Tokyo, Japan) to electron transparency. TEM was carried out in a JEOL JEM-2100HR microscope (JEOL, Tokyo, Japan) at 200 kV to determine morphology, crystalline structure and elemental composition of the sub-micrometer features of the aluminum alloy. For TEM imaging and electron diffractions the Gatan Orius SC 1000 CCD camera (Pleasanton, California, USA) was used and for elemental composition TEM or STEM with bright-field (BF) and dark-field (DF) detectors were used, combined with energy dispersive x-ray spectroscopy (EDS) with JED-2300 (JEOL, Tokyo, Japan) for point and line analyses, and elemental mappings. Elemental mappings were recorded from around 30 min to almost 2 h, depending on the area of the analysis and analysis conditions.

3. Results and discussion

3.1. Natural aging

3.1.1. Hardness evolution

The hardness evolution during natural aging reveals an enhanced hardness increase with aging time. For the sample groups with lower homogenization temperature (Fig. 2(a)), a significant difference in hardness of 6 HB between the samples with and without DCT is already visible after 6 days of aging, despite the similar hardness values after 1 day of aging (around 76.5 HB). The initial difference between the samples is sustained throughout the remaining aging up to 28 days. Furthermore, the samples with 48 h exposure to liquid nitrogen (DCT 48 h) display a slightly faster hardness increase compared to the 24 h counterparts (DCT 24 h), which also yields a higher final hardness. In contrast to the first group, the group with higher homogenization temperature (Fig. 2(b)) displays a considerably lower impact of DCT on hardness development. The samples with and without DCT display a very similar hardness up to 14 days. Afterwards the DCT samples display a slightly higher hardness (about 2–3 HB) up to 28 days. The general tendency of increased hardness with DCT immersion time is not recognizable for this sample group. By comparison of both sample groups, it is clear that the homogenization temperature has a considerable influence on the DCT effect on aging process of aluminum alloy EN AW 6026. Additionally, the less homogenized state (lower homogenization temperature) allows the development of higher hardness compared to the more homogenized state, when DCT is applied. In contrast, when DCT is not applied, the hardness development as well as the maximum hardness of the alloy is very similar for both homogenization temperatures (compare w/o DCT curves of Fig. 2(a) and (b)).

3.1.2. Microstructural investigation

The microstructure evolution supports the finding of the hardness measurements that indicate a clear tendency of increased precipitation of additional phases with additional DCT processing of sample group with lower homogenization temperature (sample group A). The initial microstructures directly after homogenization of sample group A, presented in Fig. 3(a) and (b), provide evidence that the distribution and size of intermetallic phases and precipitates are similar for all the differently treated samples before the aging process. The microstructure consists of Bi-Mg-Pb melt droplets that are present in the microstructure in a random fashion. Additionally, intermetallic Al-Mn-Fe-Si phases are present in the microstructure. The general microstructural features are visible and marked in the supplied optical micrographs in Fig. 3(a). The smaller precipitates (better observable in Fig. 3(b)) display a general homogeneous distribution across the material with occasional absence patches forming in certain prior α-Al grains. The patches originate from the inhomogeneous alloying distribution and alloying depletion in the Al matrix formed by the limited homogenization and rapid quenching of the material. The enhanced optical micrographs of samples after 14 days of natural aging, provided in Fig. 3(c), display a similar distribution of secondary phases for all samples and that the phases remain similar during the natural aging process. However, with comparison of w/o DCT sample to the DCT samples, the occurrence of pure absence patches is lower for DCT samples, suggesting a higher precipitation occurrence with DCT. The density of absence patches is very similar after natural aging, which suggests that the enhanced hardening is in-fact mostly originating from the denser initial precipitation and growth of sub-micron phases induced by DCT.

For sample group B, with higher homogenization temperature, the microstructure is similar to group A (compare Fig. 4(a) to (b)). Only a slight modification of the morphology of the Al-Fe-Mn-Si intermetallic phases is present for this sample group. The intermetallic phases display generally a more elongated morphology, which is related to the stronger dissolution of the intermetallic phases during the normalization procedure. The optical micrographs of the samples provide no considerable evidence of modified precipitation with application of DCT for sample group B.

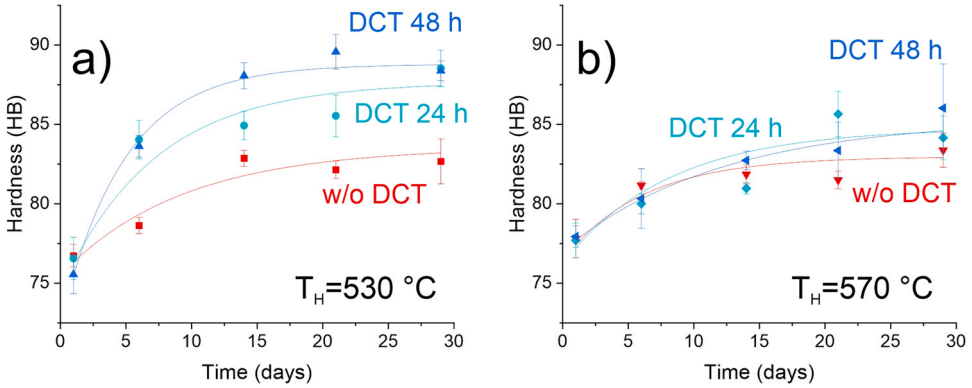

Fig. 2. Hardness change over natural aging time for differently treated samples with and without deep cryogenic treatment (DCT) with (a) lower and (b) higher homogenization temperature (T_H).

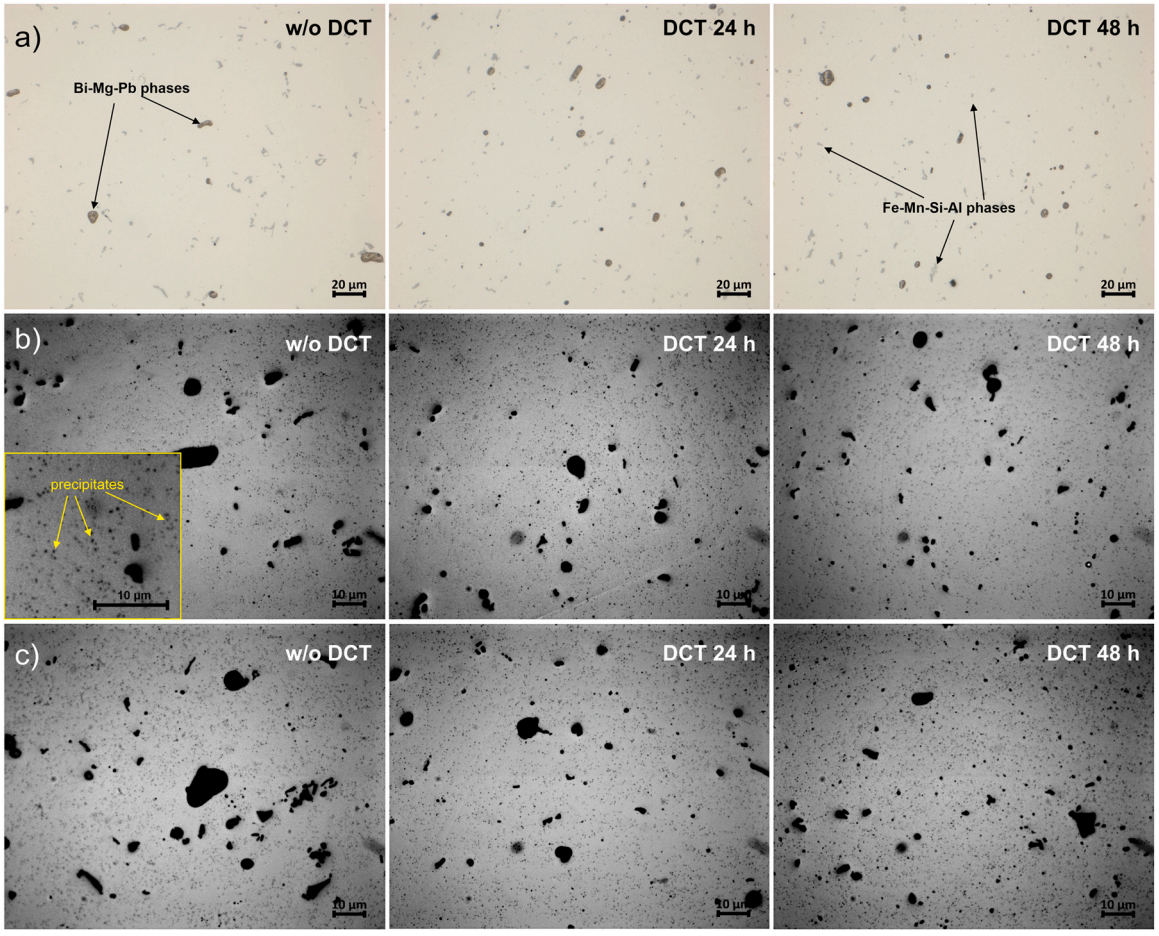

Fig. 3. (a) optical micrographs of the differently treated samples of group A after homogenization and before natural aging. (b) Contrast enhanced and refined optical micrographs of the same state of the samples as in (a). (c) Optical micrographs of the differently treated samples of group A after homogenization and 14 days of natural aging.

From SEM observations it is further confirmed that the sub-micron precipitates are more refined and more densely formed/packed for the DCT samples in comparison to the samples without DCT in the case of homogenization temperature of 530 °C (Fig. 5). As already observed from the optical micrographs, the material displays reduced amount of Al patches without presence of precipitates. All samples display an increased number of precipitates with aging time, at which DCT samples display a stronger change (best seen by comparing states after 6 days and 28 days of natural aging). The precipitates display a varying size distribution that is tendentially shifted towards smaller values for the DCT samples compared to the samples without DCT. The increase in precipitation after 28 days is determined to be in the range of 22% and 35% higher for 24 h DCT and 48 DCT, respectively, in comparison to the precipitation increase for the sample without DCT. The analysis of the distribution of sub-micron precipitates and their morphology after 28 days of natural aging (presented in Table 4) give a clear indication of the average smaller size of precipitates with increased exposure to DCT, which also induces a higher density of precipitates (see area % of Table 4). The morphology of particles, described through circularity and

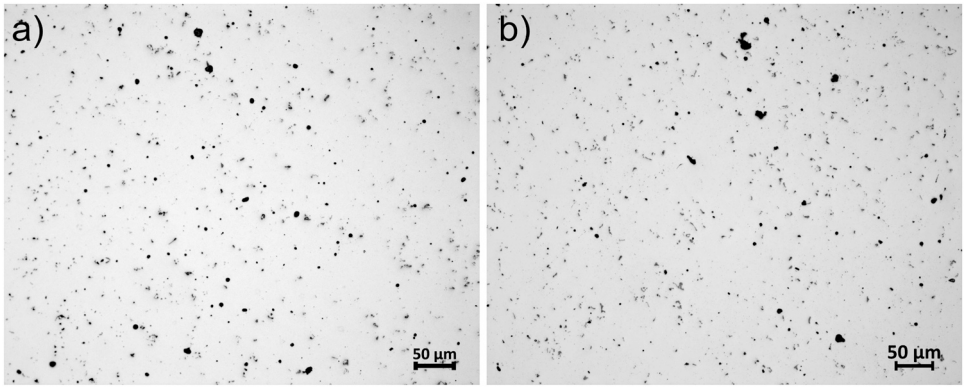

Fig. 4. Optical micrographs depicting typical microstructural features and phase distribution for (a) sample group A and (b) sample group B.

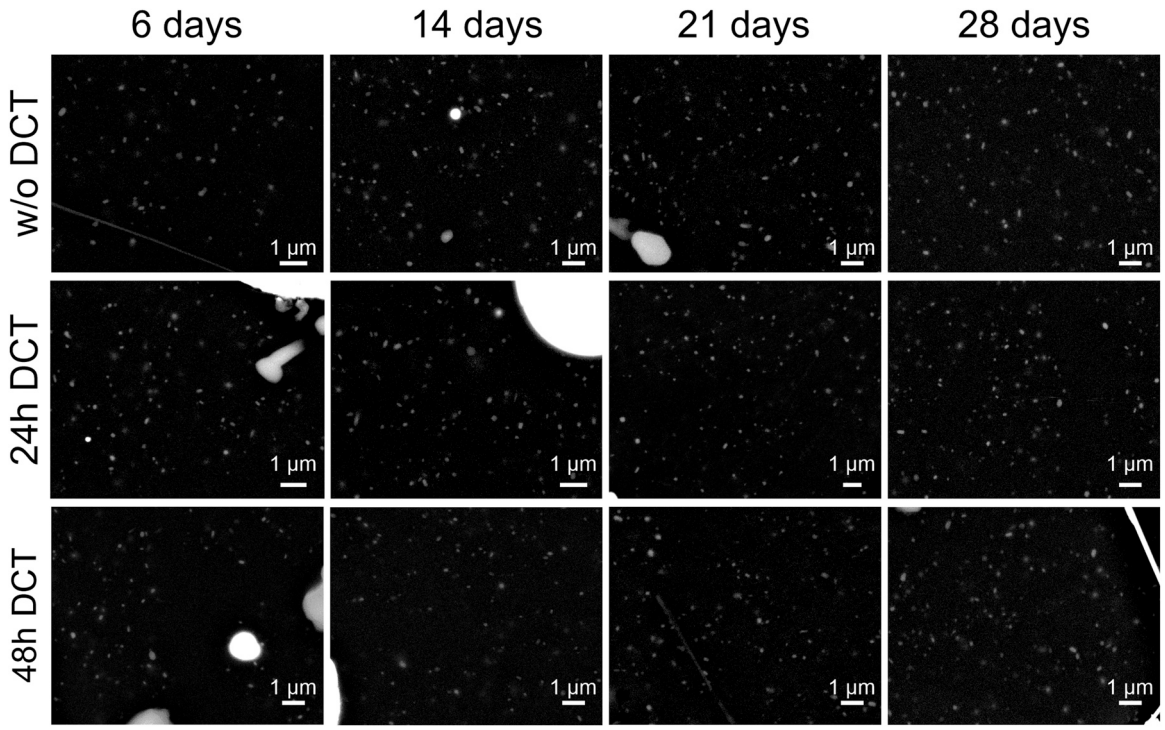

Fig. 5. SEM images of samples after natural aging for 6, 14, 21 and 28 days with homogenization temperature of 530 °C. The presented sample regions are representative displays of the average precipitation occurrence for individual samples at specific natural aging time.

Table 4
Extracted values of sub-micrometer precipitates analysis for all naturally aged samples performed on SEM images on a representative area of 96 × 80 µm^2. The area % represents the amount of area occupied by precipitates. The circularity represents the fraction of the particle shape towards a perfect circle, whereas solidity represents the filling of a convex area around a particle.

Homogenization temperature	Sample	Average size (nm^2)	Area %	Circularity	Solidity	Skewness	Kurtosis
530 °C	w/o DCT 28 days	21300	3.585	0.520	0.726	0.445	0.048
	24 h DCT 28 days	20200	3.695	0.526	0.737	0.462	0.115
	48 h DCT 28 days	19400	3.940	0.504	0.723	0.431	0.008
570 °C	w/o DCT 28 days	22500	2.114	0.425	0.674	0.460	0.042
	24 h DCT 28 days	21300	2.150	0.456	0.697	0.436	-0.183
	48 h DCT 28 days	19900	2.570	0.503	0.719	0.452	-0.019

solidity, and their distribution analysis, described through skewness and kurtosis (Table 4), indicate a similar morphology and distribution of precipitates between the different samples.

For sample group B, with higher homogenization temperature, the average precipitate size is also reduced with longer exposure to DCT (Table 4). However, the average precipitate size is larger for the samples of group B in comparison to the equivalent samples of group A. The density of precipitates is also similarly increasing with increased DCT exposure as observed for group A, with the average density being lower for samples of group B compared to the other group. The morphology of the particles indicates a different trend as observed for the first group, as both the circularity and solidity of the precipitates increases with DCT exposure, indicating rounder precipitates with DCT. The distribution of precipitates, described through the kurtosis and skewness, is for all samples similar, which indicates similar precipitation and growth of precipitates for all samples. Based on the results of both groups it is clear that DCT does indeed modify the precipitation behavior of the material with respect to increased nucleation. However, the growth of precipitates during natural aging is influenced differently based on selected homogenization temperature. While for sample group A, the growth of smaller precipitates is clearly visible from SEM images, for group B the growth of precipitates is not visible. The exemplar set of images presented in Fig. 6 provides direct evidence of the similar precipitates size and density with natural aging time for samples without and with DCT and the lack of growth of smaller precipitates as determined for group A.

The lack of precipitate growth for group B can be explained through the different homogenization of the alloy. Based on thermodynamic calculations (see) the homogenization at 570 °C allows the complete dissolution of prior Mg_2Si and reduction of other precipitates and intermetallic phases. As a result, the fraction of precipitates is reduced and alloying of matrix aluminum with Si is increased compared to the matrix material with homogenization at 530 °C (see). Another, considerably unexpected, feature of the homogenization at 570 °C is the modification of the Bi phase present in the Bi-Mg-Pb melt drops (compare Fig. 7(a) to Fig. 7(b)) that are randomly dispersed throughout the material and have separated two-phase structure with pure Pb phase and Mg-Bi phase [41]. The Bi phase at higher homogenization temperature of 570 °C develops small precipitating structures (Fig. 7(b)) that are confirmed to be Mg3Bi2 (based on local chemical analysis with EDS and data from Bi-Mg phase diagram [42]). The induced precipitation consumes the Mg from the solid solution of Bi-Mg regions, which in turn depletes the matrix of Mg (see Table 5). As a result, the reduced content of Mg constricts the precipitation and growth of Mg2Si and other precipitates. In turn, the matrix is thus enriched with Si, which is exerted from the matrix as pure Si plate-like particles during the

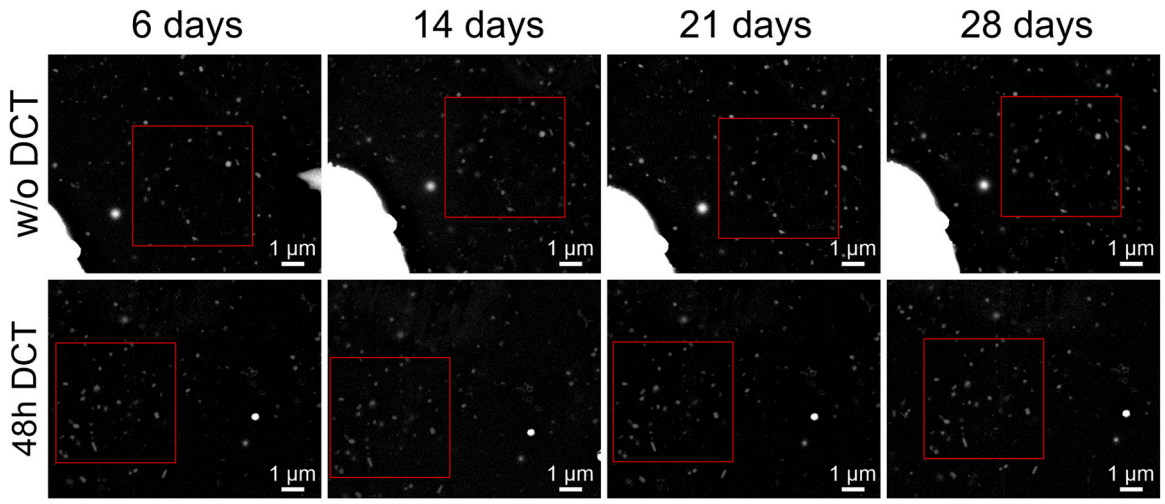

Fig. 6. SEM images of samples after natural aging for 6, 14, 21 and 28 days with homogenization temperature of 570 °C. The presented sample regions are representative displays of the average precipitation occurrence for individual samples at specific natural aging time. The red boxes indicate the region of interest of identical precipitates monitored throughout the natural aging process. (For interpretation of the references to colour in this figure legend, the reader is referred to the web version of this article.)

homogenization at 570 °C (Fig. 7(c)). In contrast, the samples homogenized at 530 °C do not display the formation of such Si particles. The feasibility of such behavior is confirmed through the thermodynamically calculated phase diagram of the system in dependency of temperature and Mg variation (Fig. 7(d)). The phase diagram displays that the development of Si particles occurs at value of < 0.5 at% of Mg, which is a considerably feasible concentration level that could be present in the pure Al matrix within the probed matrix area (Table 5) that is constructed of the pure Al matrix and

Table 5
Chemical composition determined with energy dispersive X-ray spectroscopy (EDS) of the matrix material of samples prepared with different homogenization temperature. Each value and its standard deviation are determined on 5 representative areas of the matrix material from 3 separate samples for each temperature group.

Homogenization temperature	Mg in matrix (at%)	Si in matrix (at%)
530 °C	0.94 ± 0.05	0.96 ± 0.14
570 °C	0.78 ± 0.05	0.89 ± 0.12

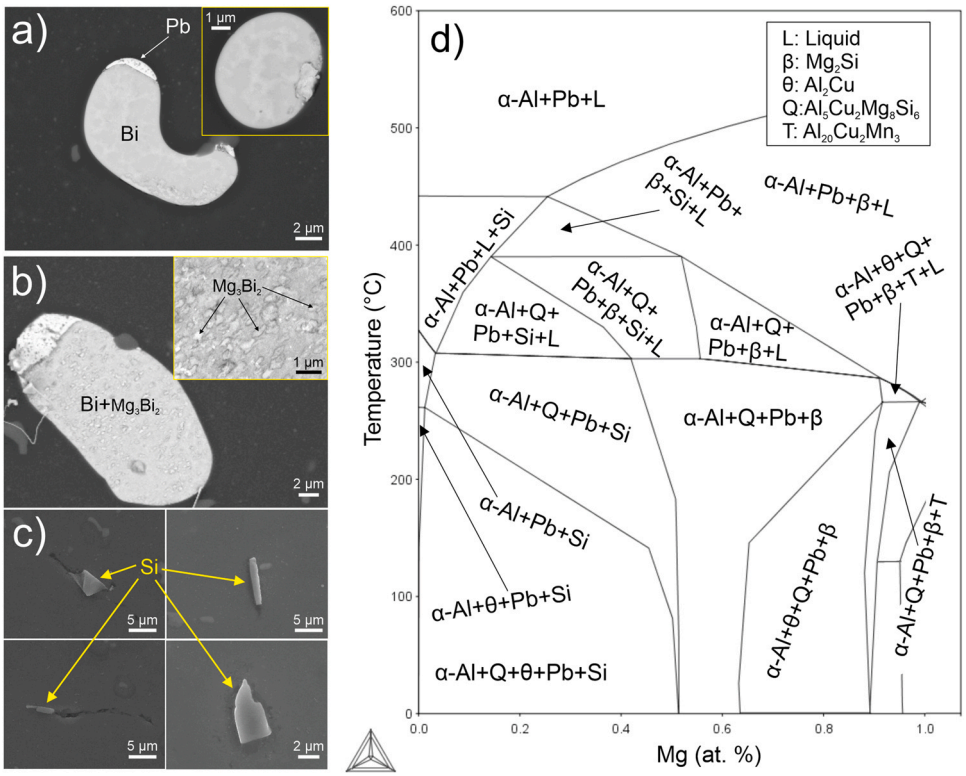

Fig. 7. Scanning electron microscopy micrographs of Bi-Mg-Pb melt drops for (a) samples homogenized at 530 °C and (b) samples at 570 °C. The insert of (a) represents another smaller melt drop without the Pb phase. The insert of (b) represents the enlarged portion of the Bi region indicating the precipitation of additional Mg_3Bi_2 phase. In (c) images of present Si particles of various morphologies formed in samples homogenized at 570 °C. (d) Equilibrium phase diagram of the investigated alloy calculated in dependency of varying Mg content. The Bi and Fe holding phases are not presented for simplification of the phase diagram presentation.

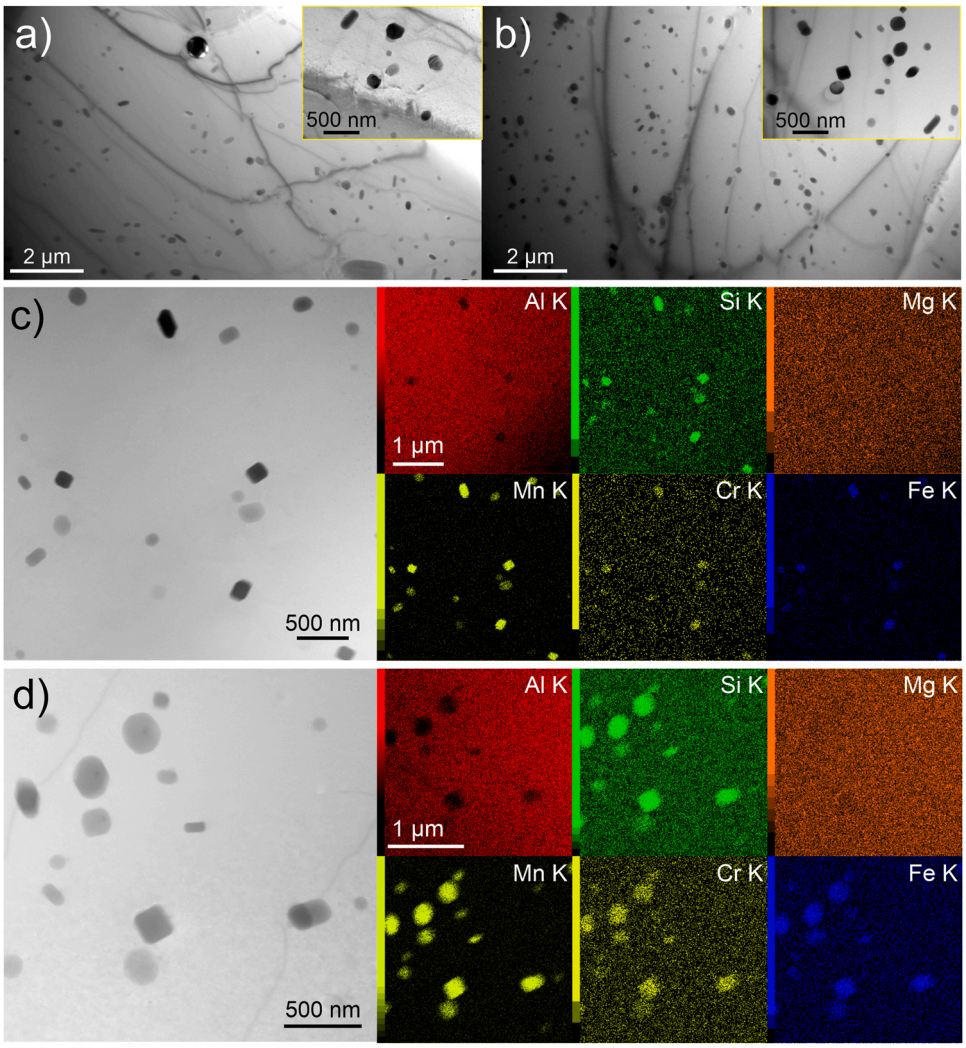

Fig. 8. Transmission electron microscopy images of naturally aged samples (a) without DCT and (b) with 48 h exposure to DCT homogenized at 530 °C. The inserts in (a) and (b) are enlarged micrographs depicting the different dispersoids present in both samples. For both samples (c) without DCT and (d) with 48 h exposure to DCT homogenized at 530 °C, selected regions with dispersoids and corresponding energy dispersive X-ray spectroscopy maps of selected elements are presented.

submicron precipitated particles. As a consequence, the Si and Mg depleted matrix results in a general reduced formation of Mg2Si precipitates and other precipitates. Furthermore, the distribution of alloying elements is considerably more homogenized at 570 °C (see), which generally reduces the possibility of precipitate regrowth through chemical inhomogeneity and local agglomeration of alloying elements. From the acquired data it can be concluded that the depleted matrix and higher homogeneity of the alloy leads to reduced precipitation from the matrix, which translates to a generally lower hardness with aging and also significantly lower effectiveness of DCT on additional precipitation with natural aging.

From the SEM micrographs, it is visible that the sub-micrometer particles range in size and morphology, which suggest that the precipitates are most probably of different chemical composition and structure. The calculated phase diagram (Fig. 7(d)) indicates that additionally to Mg_2Si (β-phase) also Al_2Cu (θ-phase) and other more complex phases such as $Al_5Cu_2Mg_8Si_6$ (Q-phase) and $Al_{20}Cu_2Mn_3$ (T-phase) can be present in the system as precipitates. Furthermore, the general expectation of natural aging of 6xxx alloys is also the development of β'' and β' phases, which can play a decisive role in the aging of the alloy [30]. As shown by TEM and STEM analysis (Fig. 8) the precipitates are clearly of different morphology and size. The DCT samples have an increased amount of precipitates that is visible by comparing the exemplar TEM images of sample without DCT in Fig. 8(a) to sample with 48 h DCT in Fig. 8(b). All samples hold the different types of precipitates, at which the DCT samples generally hold more smaller precipitates of rounder form compared to the sample without DCT. With EDS mapping (presented in Fig. 8(c) and (d)) and point EDS analysis, the larger precipitates are confirmed as α-$Al_{15}(Fe,Mn)_3Si_2$ dispersoids that either formed during the homogenization of the alloy or are residuals of the prior microstructure before homogenization. However, the smaller and more rounder precipitates are chemically different to the larger dispersoids by reduced amount of Cr, Si, Mn and Fe, which is visible from the EDS maps. This is possibly related to the size of the particles themselves, however, the ratio of Si to (Fe,Mn) is smaller in these particles, with most of the particles displaying a ratio of 1:2 in contrast to the larger particles that have a ratio of 2:3. This suggests that the particles are most probably a result of the residual presence of heavier alloying elements (Fe, Mn and Cr) of the prior partially dissolved dispersoids after homogenization that are situated in the vicinity of the prior dispersoid location. Afterwards these elements agglomerate and the particles regrow during natural aging to a certain extent based on the local chemical potential and residual structures and chemistry of the surrounding area. As the Si is much more diffusive than the other alloying elements and incorporates itself into the matrix and local GP-zones, the deficit in Si occurs upon the regrowth of the rounder dispersoid particles.

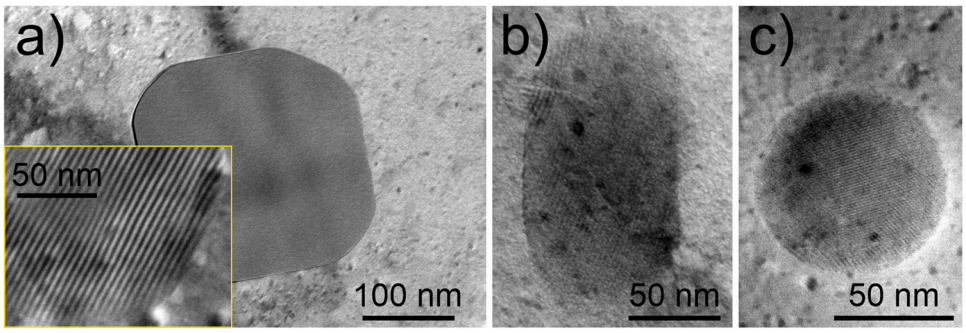

Fig. 9. Transmission electron microscopy images of dispersoids found in naturally aged samples. (a) Depicts a large dispersoid with incoherent boundaries and no sign of dissolvement of the particle into the matrix. The insert depicts the boundary of the dispersoid with the matrix. (b) Represents a smaller dispersoid that displays gradual dissolvement of the particle into the matrix material. (c) Displays a reformed spherical dispersoid with a surrounding ring of depleted matrix material.

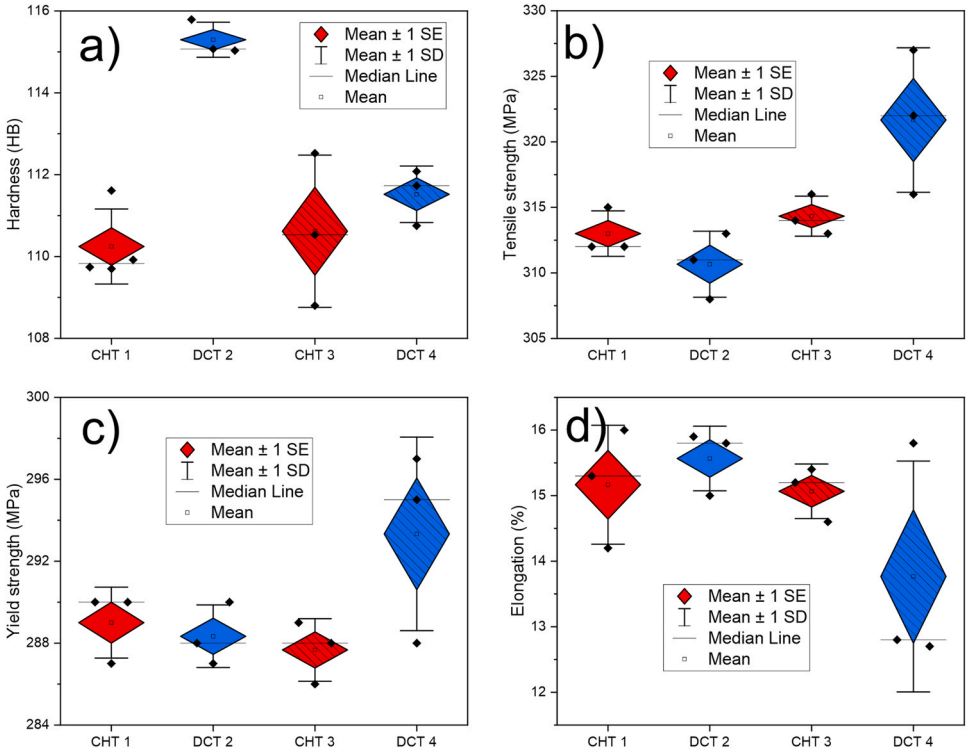

Fig. 10. (a) hardness, (b) tensile strength, (c) yield strength and (d) elongation of artificially aged samples. The box represents the standard error (SE) and the whiskers represent the standard deviation (SD).

Based on the above explanation, the higher density of smaller and rounder particles for DCT samples compared to the sample without DCT can be explained. It is proposed that DCT induces lowering of the diffusional barriers of the atomic migration and reformation of the alloying elements through compressive stress inhibition and dislocation density modification. The exposure to liquid nitrogen temperatures has been proven to reduce the residual tensile stresses of aluminum alloys [13,43,44], which is also considered to be related to the modification of the dislocation density [43]. This could well be the reason for the sudden and considerably stronger modification of the growth of dispersoids with DCT for samples with homogenization temperature of 530 °C. Such mechanism also explains the more rounded formation of the smaller reoccurring dispersoids (example in Fig. 9(c)), as the growth process is related to a homogeneous agglomeration of surrounding alloying elements without activating preferential atom migration towards lower energy facets and directions. The indication for such behavior is given by TEM images that disclose a brighter contrast around the reformed spherical dispersoids, which suggests a local depletion of the matrix material of alloying elements (see Fig. 9(c)). Such behavior also explains the considerably lower effect of DCT on the enhancement of natural aging of sample group B, since the homogenization at higher temperature allows higher dissolvement of the dispersoids (example in Fig. 9(b)) and with it also a more homogenous distribution of dissolved alloying elements away from the dispersoids prior positions. As a result, the raised driving force of atom migration with DCT cannot have such an influence as the agglomeration of particles is considerably less at homogenization temperature of 570 °C compared to 530 °C (see). As a result, only the larger dispersoids with strong incoherent grain boundaries will generally remain in the case of samples without DCT treatment (example in Fig. 9(a).

These results and explanation indicate that the dispersoids are the main phases for the increase of the hardness with prolonged natural aging time with DCT. Based on the fact that no clear precipitation of other particles is visible, it is concluded that the hardness growth in CHT samples is mainly related to the formation of smaller GP-zones and initial β'' phases, which have been proven to form for Al-Mg-Si alloys during natural aging [25], also with DCT

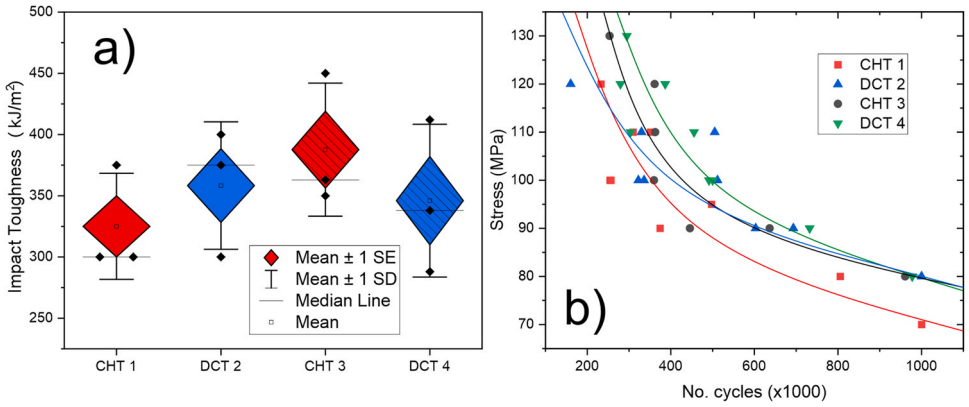

Fig. 11. (a) Impact toughness and (b) S-N curve for fatigue properties of artificially aged samples. For impact toughness the box represents the standard error (SE) and the whiskers represent the standard deviation (SD).

[16]. However, with DCT the dispersoids play an additional role through a subprocess of reformation and regrowth, which increases the density and size of the dispersoids as well as modifies their coherency with the matrix. As a result, the hardness increases further due to dislocations interaction with dispersoids through Orowan bowing and looping (see), which also leads to a considerably higher hardness value than normally found for similar alloys during natural aging [45–47]. Furthermore, the presented results also indicate that possibly the hardness increase during natural aging could be partially a result of the dispersoids reforming also in the case of CHT samples, since the rounder dispersoids with coherent/semi-coherent boundaries are also present in the CHT samples, but in considerably lower quantity.

3.2. Artificial aging

3.2.1. Mechanical properties

The selected artificial aging indicates that DCT has a positive influence on hardness (Fig. 10(a)) in the case of lower homogenization temperature (compare CHT 1 to DCT 2), whereas in the case of higher homogenization temperature the hardness levels are within the same range (compare CHT 3 to DCT 4). Contrary, the tensile properties are negligibly altered with DCT, when artificial aging is performed for samples with homogenization temperature of 530 °C (Fig. 10 (b)-(d)). Whereas for the second group the tensile strength (Fig. 10 (b)) and yield strength (Fig. 10 (c)) are raised with DCT and with it proportionally the elongation Fig. 10 (d)) is reduced. Similarly as for the natural aging, these basic mechanical properties indicate that the homogenization temperature influences the DCT effect on the artificial aging of the two sample groups. The surprising feature of DCT effect for the first group is the increased hardness and simultaneous reduced tensile strength. Such behavior connected with the significantly higher hardness of the alloy in comparison to naturally aged samples indicates that the precipitation of β-type particles must be present. For the second group, the surprising feature is the differently behaving tensile properties of the DCT samples that display higher strength, but also a strong scattering of the properties from sample to sample in comparison to CHT samples (see). Based on the microstructural research of previous, naturally aged, samples, the possible cause could be in the formation of Si particles that have a high notch effect, leading to higher chance of sudden failure with denser and finer precipitation for DCT samples.

The impact toughness measurements, shown in Fig. 11 (a), indicate a slight increase in the mean value with DCT for lower homogenization temperature, whereas with higher homogenization temperature a slight deterioration of the property occurs with DCT. However, for both sample groups, DCT displays a negligible effect on the impact toughness, when scattering of the results is considered. Despite this, the obtained S-N curves from fatigue testing (Fig. 11 (b)) show a clear trend of improved fatigue resistance for DCT samples compared to their CHT counterparts. In the case of the first group, the S-N curve is shifted towards higher stress amplitudes for the DCT sample, which is well pronounced in the range from 400,000 to 1000,000 cycles. In contrast, the second group with higher homogenization temperature displays a less distinct improvement, which is only visible in the range from 300,000 to 600,000 cycles. The significant improvement of the DCT sample as well as the modified shape of the S-N curve for the first group of samples correlates well with the simultaneous increase in hardness and impact toughness of the material. In the second group, the fatigue improvement at lower number of cycles is considered to be a result of the higher tensile strength after DCT that translates to higher resistance to fatigue at high loads.

3.2.2. Microstructural investigation

The SEM observations (Fig. 12) reveal, similarly as for the naturally aged samples, that DCT samples (Fig. 12 (b) and (d)) display an increased number of dispersoids in contrast to their CHT counterparts (Fig. 12 (a) and (c)), regardless of the selected homogenization temperature. However, in contrast to the naturally aged samples, the artificially aged samples generally display a similar amount of submicrometer dispersoids with respect to the different homogenization temperatures for both CHT (compare (a) to (c) in Fig. 12) and DCT (compare (b) to (d) in Fig. 12) samples. This indicates that the increased temperature of aging allows the development of the dispersoids in a similar manner for both sample groups, irrespective of the homogenization temperature.

The DCT samples generally display on average a more acicular dispersoid formation, which was also confirmed with TEM (Fig. 13 (a)-(b)). Similarly, TEM also confirms the increased amount of dispersoids for DCT samples in comparison to the CHT samples. The DCT samples display a general formation of dispersoids with elongated morphologies oriented mostly along the < 100 > axes of the Al matrix. The elongated dispersoids with the same preferential orientation are also present for the CHT samples, but in a smaller quantity and with a generally shorter length. Additionally, both CHT and DCT samples still display spherical and cuboidal dispersoids of different size, with the DCT samples exhibiting more spherically-shaped dispersoids rather than cuboidal. The chemical analysis of the individual dispersoids indicate a general reduction of alloying with Cr and Fe. The spherical and elongated dispersoids display also a reduced amount of Si and Mn, at which the ratio between the two elements ranges from 1:2, as observed for the spherical dispersoids during natural aging, to a ratio of 1:1. For the elongated dispersoids,

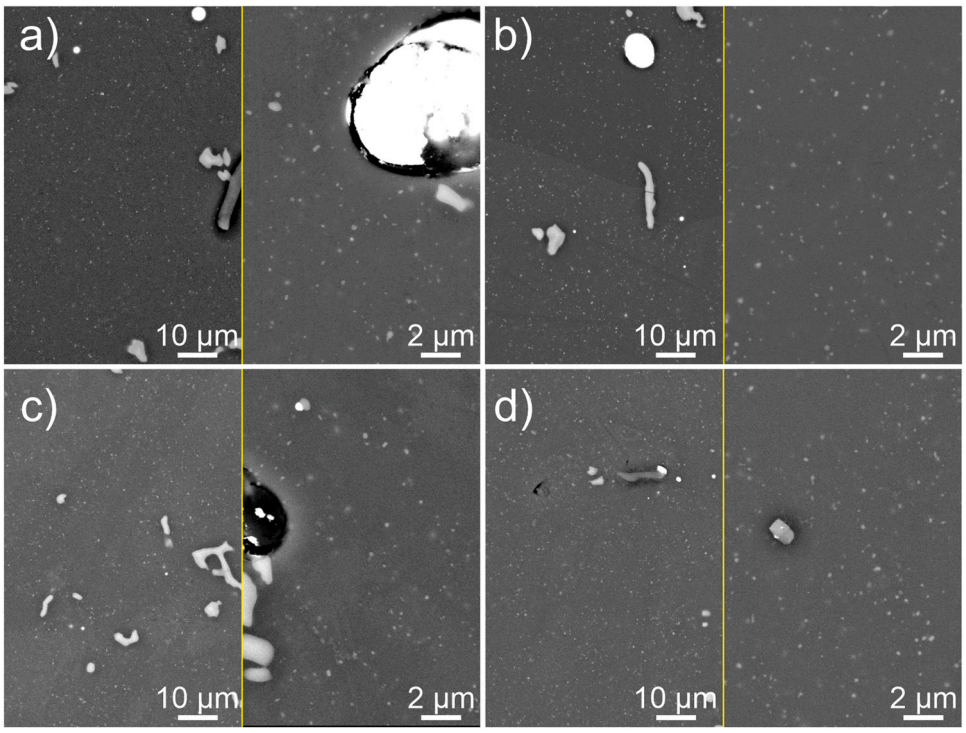

Fig. 12. SEM images of samples after artificial aging for conventionally heat treated ((a) and (c)) and deep cryogenic treated samples ((b) and (d)) with different homogenization temperatures of 530 °C ((a) and (b)) and 570 °C ((c) and (d)). The images provide representative images of the microstructure at two different magnifications for each sample.

this chemical ratio differs across the length from point to point and displays a Si enriched spherical central zone. The zone is associated to the residual position and shape of the prior dispersoid, from which the elongated particle grew. An example of such a structure is visible from the EDS maps in Fig. 13 (c). Additionally, for the CHT samples, the cuboidal dispersoids remain in their initial

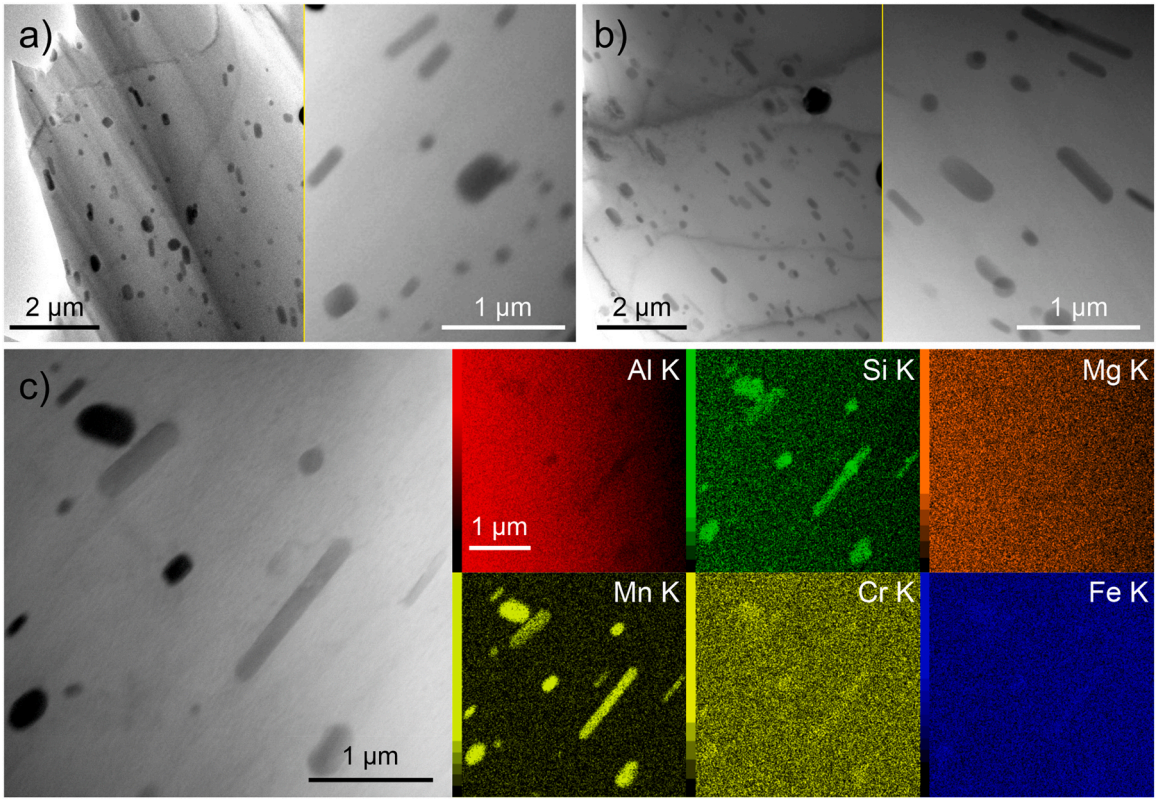

Fig. 13. Transmission electron microscopy images of artificially aged samples (a) without DCT and (b) with 48 h exposure to DCT obtained at two different magnifications to indicate the average density and morphology of dispersoids. (c) Representative region with different dispersoids and corresponding energy dispersive X-ray spectroscopy maps of selected elements, which are present in all artificially aged samples.

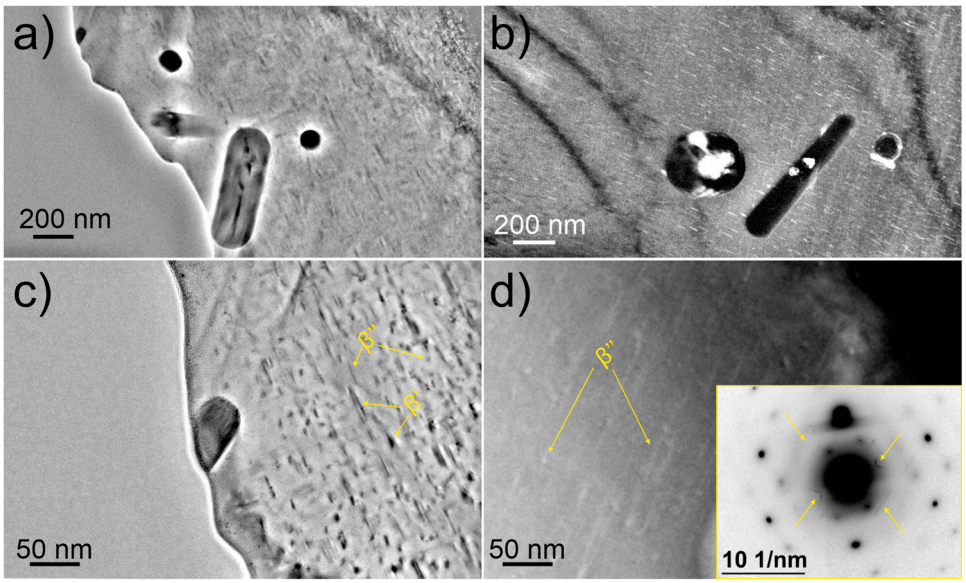

Fig. 14. Exemplar transmission electron microscopy (TEM) images of the precipitation of β'' needles for (a), (c) CHT and (b), (d) DCT samples. The insert in d) represents the corresponding selective area electron diffraction diffractogram with indicated streaks formed by the oriented β'' precipitates. For the CHT sample the TEM images are acquired with brightfield technique, whereas for the DCT sample the TEM images are acquired with darkfield technique for the visualization of the increased contrast of the precipitates along the < 100 > directions of the aluminum matrix.

stochiometric state of $Al_{15}Mn_3Si_2$, whereas the other two dispersoid types display similar stoichiometry as observed for the rounder dispersoids of naturally aged DCT samples. This suggests that DCT in-fact modifies the transitioning coherent/semi-coherent boundary (see Fig. 9(c)) by increasing the diffusivity of the alloying elements through shrinkage pressure and dislocation pile-up, which effectively reduces the energy barrier for the growth along the energetically favorable orientations of < 100 > of the aluminum matrix. In turn, the DCT samples develop longer dispersoids than the CHT samples.

The results have proven that DCT strongly modifies the change of dispersoids with aging. Nevertheless, for the artificially aged samples, DCT also promoted the change in the formation of smaller β-type particles that commonly form during artificial aging [30]. TEM observations (Fig. 14) indicate that the CHT samples display typical ladder-like formation of needle-shaped β-type particles, which can be separated into thinner β'' and thicker β' particles (marked in Fig. 14 (c)). The identification was determined based on the morphological character of the two precipitate groups as well as based on the local chemical difference of the two particle groups (compared to literature [25,30,48,49]). In contrast, the DCT samples display mainly thinner β'' (see Fig. 14 (d)) with on average higher density as well as considerably longer average length of the precipitates in comparison to those found in CHT samples (compare Fig. 14 (a) with (b)). The increased density of the β'' precipitates with DCT is again a result of the shrinkage of the material and increased amount of dislocation density. These effectively reduce the nucleation energy barrier of the precipitates, which has been confirmed with differential scanning calorimetry performed by Huang et al. [16] on a similar aluminum alloy type during natural aging. Furthermore, the increased dislocation density results in larger amount of dislocation piles that act as nucleation sites for the precipitates [50]. The precipitates for both CHT and DCT samples are aligned along the < 100 > directions of the aluminum matrix, which is resolved by the streaks formed within the selective area electron diffraction pattern (example in insert of Fig. 14 (d)). Surprisingly, the different homogenization temperatures did not reveal significant differences in the precipitation of β'' and β' particles. It is postulated that the higher hardness with DCT in the case of lower homogenization temperature is a result of the denser precipitation of β''. However, for the case of higher homogenization temperature, for which only slight hardness increase is registered, the reason could potentially lie in the depletion of Mg and Si, leading to reduced size and/or reduced netting of the precipitates [48,51]. However, these features could not be confirmed or disputed with currently used methods.

In contrast, the remaining mechanical properties seem to be unrelatable to the changes of the precipitation with DCT and furthermore no clear trend with different homogenization temperature can be established for these properties. It is possible that the additional presence of heavier alloying elements such as Fe, Mn, Cr and Zr could be inducing additional formation of low-melting complex precipitates coupled together with the Al-Si structures that can potentially change the hardening effect of these precipitates. It has been recently shown that with specific alloying of aluminum alloys, new low-melting Al-Si phases can be formed thus giving the possibility to modify the precipitation dynamics of the whole system [52] and in our case the influence of DCT. For the above-mentioned reasons, it is proposed that more research needs to be performed on this matter using more sophisticated techniques such as atomic probe tomography or small angle neutron scattering in order to establish a clear consensus on the formation and development of GP zones and β-type particles, when DCT is applied. Regardless of this, DCT is proven to have a significant impact on the aging evolution of 6xxx aluminum alloys and allows achievement of high hardness values that surpass standardly obtained hardness values and are comparable to hardness values obtained with specialized and complex heat-treatment procedures [7,46,53,54].

4. Conclusions

The research provides insight into change of the aging behavior of aluminum alloy EN AW 6026 with its exposure to deep cryogenic treatment (DCT). The microstructural results confirm changes in the precipitation and growth of sub-micrometer dispersoids, when DCT is applied before aging. Additionally, the work provides the first research and first evidence of the effect of DCT on dispersoids. With DCT the dispersoids reform their shape from a preferential cuboidal

shape to a more spherical form during natural aging and during artificial aging the dispersoids and β'' precipitates become more elongated. Additionally, DCT induces denser formation of dispersoids and β'' precipitates as well as retards the growth of larger β' precipitates. The changes are associated with the improved diffusivity of alloying elements.

However, the effectiveness of DCT is strongly dependent on the homogenization temperature. The higher (570 °C) homogenization temperature results in a significant reduction of the hardness improvement for DCT in comparison to the lower (530 °C) homogenization temperature. This originates from the precipitation of Mg_3Bi_2 in the accompanied Bi phases, which result in Mg and Si depletion of the matrix and with-it retarded development of dispersoids and precipitates.

Due to the microstructural changes, the hardness change during natural and artificial aging is amplified with the application of DCT. The duration of exposure to DCT (from 24 to 48 h) also increases the impact of DCT on the hardness evolution during natural aging, increasing both the hardening rate and maximal level of achieved hardness. Additionally, DCT yields improved fatigue resistance, especially with lower homogenization temperature, as well as increased strength, observed for samples with higher homogenization temperature. As such the modification of mechanical properties after artificial aging with DCT can be partially related to denser precipitation of β'' particles and matrix depletion of Mg and Si, but some correlations remain unclear. As a result, further, more sophisticated, investigations of the DCT effect on artificially aged Al-Mg-Si alloys are required to underline the main contributions of DCT on GP zones and development of β-type precipitates during artificial aging.

Funding

This work was supports by Slovenian Research Agency (ARRS) [J2–9211 and P2–0050].

CRediT authorship contribution statement

M.J.-K.: Investigation, Modeling, Visualization, Conceptualization, Data curation, Formal analysis, Writing – original draft, Writing – review and editing. **R.R.**: Investigation, Visualization, Writing – original draft, Writing – review and editing. **P.J.-K.**: Investigation, Modeling, Conceptualization, Writing – original draft, Writing – review and editing. **B.P.**: Conceptualization, Supervision, Writing – review and editing.

Declaration of Competing Interest

The authors declare that they have no known competing financial interests or personal relationships that could have appeared to influence the work reported in this paper.

Acknowledgements

Authors would like to thank IMT mechanical lab (G. Puš and B. Žužek), metallographic lab (N. Lipovšek), scanning electron microscope operator (T. Sever) and transmission electron microscope operator (D. Feizpour).

Appendix A. Supporting information

Supplementary data associated with this article can be found in the online version at doi:10.1016/j.jallcom.2021.163323.

References

[1] D.H. Park, S.W. Choi, J.H. Kim, J.M. Lee, Cryogenic mechanical behavior of 5000- and 6000-series aluminum alloys: issues on application to offshore plants, Cryog. (Guildf.) 68 (2015) 44–58, https://doi.org/10.1016/j.cryogenics.2015.02.001
[2] M. Lech-Grega, W. Szymañski, B. Płonka, S. Boczkal, M. Gawlik, M. Bigaj, P. Korczak, The Structure and Properties of Wrought Aluminium Alloys Series 6xxx with Vanadium for Automotive Industry, Light Met. 2013, John Wiley & Sons, Inc, Hoboken, NJ, USA, 2013, pp. 527–532, https://doi.org/10.1002/9781118663189.ch90
[3] V.F. Steier, E.S. Ashiuchi, L. Reißig, J.A. Araújo, Effect of a deep cryogenic treatment on wear and microstructure of a 6101 aluminum alloy, Adv. Mater. Sci. Eng. (2016) (2016), https://doi.org/10.1155/2016/1582490
[4] L. Mei, X.P. Chen, G.J. Huang, Q. Liu, Improvement of mechanical properties of a cryorolled Al-Mg-Si alloy through warm rolling and aging, J. Alloy. Compd. 777 (2019) 259–263, https://doi.org/10.1016/j.jallcom.2018.11.012
[5] J.R. Zhao, F.Y. Hung, B.J. Chen, Effects of heat treatment on a novel continuous casting direct rolling 6056 aluminum alloy: cold rolling characteristics and tensile fracture properties, J. Mater. Res. Technol. 11 (2021) 535–547, https://doi.org/10.1016/j.jmrt.2021.01.037
[6] Y. Liu, X. Zhao, J. Li, L. Bhatta, K. Luo, C. Kong, H. Yu, Mechanical properties of rolled and aged AA6061 sheets at room-temperature and cryogenic environments, J. Alloy. Compd. 860 (2021) 158449, https://doi.org/10.1016/j.jallcom.2020.158449
[7] F. Schmid, P. Dumitraschkewitz, T. Kremmer, P.J. Uggowitzer, R. Tosone, S. Pogatscher, Enhanced aging kinetics in Al-Mg-Si alloys by up-quenching, Commun. Mater. 2021 21 (2) (2021) 1–12, https://doi.org/10.1038/s43246-021-00164-9
[8] P. Baldissera, C. Delprete, Deep cryogenic treatment: a bibliographic review, Open Mech. Eng. J. 2 (2008) 1–11, https://doi.org/10.2174/1874155×00802010001
[9] P. Jovičević-Klug, B. Podgornik, Review on the Effect of Deep Cryogenic Treatment of Metallic Materials in Automotive Applications, Metals 10 Basel, 2020, p. 434, https://doi.org/10.3390/met10040434
[10] D. Senthilkumar, Cryogenic Treatment:Shallow and Deep, in: G.E. Totten, R. Colas (Eds.), Encycl. Iron, Steel, Their Alloy, Taylor and Francis: NY, USA, New York, NY, 2016, pp. 995–1007, https://doi.org/10.1081/E-EISA-120052805
[11] P. Mukhopadhyay, Alloy designation, processing, and use of AA6XXX series aluminium alloys, ISRN Met. 2012 (2012) 1–15, https://doi.org/10.5402/2012/165082
[12] S. Krymskiy, O. Sitdikov, E. Avtokratova, M. Markushev, 2024 aluminum alloy ultrahigh-strength sheet due to two-level nanostructuring under cryorolling and heat treatment, Trans. Nonferrous Met. Soc. China (Engl. Ed. 30 (2020) 14–26, https://doi.org/10.1016/S1003-6326(19)65176-9
[13] M. Araghchi, H. Mansouri, R. Vafaei, Y. Guo, A novel cryogenic treatment for reduction of residual stresses in 2024 aluminum alloy, Mater. Sci. Eng. A. 689 (2017) 48–52, https://doi.org/10.1016/J.MSEA.2017.01.095
[14] S. Gao, Z. Sheng Wu, P. Fei Jin, J. Jie Wang, P. Shuai, Effect of deep cryogenic treatment on microstructure of 5A06 aluminum alloy MIG welded joint, Mater. Sci. Forum, Trans. Tech. Publ. Ltd (2012) 182–185, https://doi.org/10.4028/www.scientific.net/MSF.724.182
[15] S. Bouzada, F. Cabeza, M. Merino, P, Trillo, Effect of deep cryogenic treatment on the microstructure of an aerospace aluminum alloy, Adv. Mater. Res 445 (2012) 965–970, https://doi.org/10.4028/www.scientific.net/AMR.445.965
[16] Yuanchun Huang, Y. Li, X. Ren, Z. Xiao, Effect of deep cryogenic treatment on aging processes of Al–Mg–Si alloy, Phys. Met. Met. 120 (2019) 914–918, https://doi.org/10.1134/S0031918×19070111
[17] P. Sonia, V. Verma, K.K. Saxena, N. Kishore, R.S. Rana, Effect of cryogenic treatment on mechanical properties and microstructure of aluminium 6082 alloy, Mater. Today Proc. Elsevier Ltd, 2020, pp. 2248–2253, https://doi.org/10.1016/j.matpr.2020.02.488
[18] W. Gao, X. Wang, J. Chen, C. Ban, J. Cui, Z. Lu, Influence of Deep Cryogenic Treatment on Microstructure and Properties of 7A99 Ultra-High Strength Aluminum Alloy, Metals 9 Basel, 2019, p. 631, https://doi.org/10.3390/met9060631
[19] K.E. Lulay, K. Khan, D. Chaaya, The effect of cryogenic treatments on 7075 aluminum alloy, J. Mater. Eng. Perform. 11 (2002) 479–480, https://doi.org/10.1361/105994902770343683
[20] L. Wei, D. Wang, H. Li, D. Xie, F. Ye, R. Song, G. Zheng, S. Wu, Effects of cryogenic treatment on the microstructure and residual stress of 7075 aluminum alloy, Metals 8 (2018) 1–10, https://doi.org/10.3390/met8040273
[21] Z. Weng, X. Xu, B. Yang, K. Gu, L. Chen, J. Wang, Cryogenic thermal conductivity of 7050 aluminum alloy subjected to different heat treatments, Cryog. (Guildf.) 116 (2021) 103305, https://doi.org/10.1016/j.cryogenics.2021.103305
[22] Y. Wang, Z. Jiang, Dynamic compressive behavior of selected aluminum alloy at low temperature, Mater. Sci. Eng. A. 553 (2012) 176–180, https://doi.org/10.1016/j.msea.2012.06.010
[23] Y.B. Lee, D.H. Shin, K.T. Park, W.J. Nam, Effect of annealing temperature on microstructures and mechanical properties of a 5083 Al alloy deformed at cryogenic temperature, Scr. Mater. 51 (2004) 355–359, https://doi.org/10.1016/j.scriptamat.2004.02.037
[24] O. Adem, Effects of artificial aging heat treatment on mechanical properties and corrosion behaviour of AA6XXX aluminium alloys, J. Chem. Eng. Mater. Sci. 9 (2018) 17–23, https://doi.org/10.5897/jcems2018.0315

[25] R. Vissers, M.A. van Huis, J. Jansen, H.W. Zandbergen, C.D. Marioara, S.J. Andersen, The crystal structure of the β′ phase in Al-Mg-Si alloys, Acta Mater. 55 (2007) 3815–3823, https://doi.org/10.1016/j.actamat.2007.02.032
[26] A. Poznak, V. Thole, P. Sanders, The Natural Aging Effect on Hardenability in Al-Mg-Si: A Complex Interaction between Composition and Heat Treatment Parameters, Metals 8 Basel, 2018, p. 309, https://doi.org/10.3390/met8050309
[27] J.D. Robson, O. Engler, C. Sigli, A. Deschamps, W.J. Poole, Advances in microstructural understanding of wrought aluminum alloys, Metall. Mater. Trans. A 2020 519 (51) (2020) 4377–4389, https://doi.org/10.1007/S11661-020-05908-9
[28] J. Pezda, A. Bielsko-Biała, The effect of the t6 heat treatment on hardness and microstructure of the EN AC-AlSi12CuNiMg alloy, Metalurgija 1 (2014) 63–66.
[29] O. Engler, O.R. Myhr, Effect of natural ageing on strength and anisotropy in aluminium alloy AA 6005C, Mater. Sci. Forum, Trans. Tech. Publ. Ltd (2017) 688–694, https://doi.org/10.4028/www.scientific.net/MSF.877.688
[30] Q. Xiao, H. Liu, D. Yi, D. Yin, Y. Chen, Y. Zhang, B. Wang, Effect of Cu content on precipitation and age-hardening behavior in Al-Mg-Si-xCu alloys, J. Alloy. Compd. 695 (2017) 1005–1013, https://doi.org/10.1016/J.JALLCOM.2016.10.221
[31] C. Sigli, F. De Geuser, A. Deschamps, J. Lépinoux, M. Perez, Recent advances in the metallurgy of aluminum alloys. Part II: Age hardening, Comptes Rendus Phys. 19 (2018) 688–709, https://doi.org/10.1016/j.crhy.2018.10.012
[32] D. Maisonnette, M. Suery, D. Nelias, P. Chaudet, T. Epicier, Effects of heat treatments on the microstructure and mechanical properties of a 6061 aluminium alloy, Mater. Sci. Eng. A. 528 (2011) 2718–2724, https://doi.org/10.1016/j.msea.2010.12.011
[33] M. Kenyon, J. Robson, J. Fellowes, Z. Liang, Effect of dispersoids on the microstructure evolution in Al – Mg – Si alloys, Adv. Eng. Mater. 21 (2019) 1800494, https://doi.org/10.1002/adem.201800494
[34] F. Hichem, G. Rebai, Study of dispersoid particles in two Al–Mg–Si aluminium alloys and their effects on the recrystallization, Appl. Phys. A Mater. Sci. Process. 119 (2015) 285–289, https://doi.org/10.1007/s00339-014-8963-5
[35] N.C.W. Kuijpers, F.J. Vermolen, C. Vuik, P.T.G. Koenis, K.E. Nilsen, S. van der Zwaag, The dependence of the β-AlFeSi to α-Al(FeMn)Si transformation kinetics in Al-Mg-Si alloys on the alloying elements, Mater. Sci. Eng. A. 394 (2005) 9–19, https://doi.org/10.1016/j.msea.2004.09.073
[36] K. Strobel, E. Sweet, M. Easton, J.F. Nie, M. Couper, Dispersoid phases in 6xxx series aluminium alloys, Mater. Sci. Forum, Trans Tech Publications Ltd, 2010, pp. 926–929, https://doi.org/10.4028/www.scientific.net/MSF.654-656.926
[37] M. Remøe, I. Westermann, K. Marthinsen, Characterization of the Density and Spatial Distribution of Dispersoids in Al-Mg-Si Alloys, Metals 9 Basel, 2018, p. 26, https://doi.org/10.3390/met9010026
[38] Y. Han, K. Ma, C. Wang, H. Nagaumi, Precipitation behavior of dispersoids in Al-Mg-Si-Cu-Mn-Cr alloy during homogenization annealing, ICAA13 Pittsburgh, Springer International Publishing, 2012, pp. 1817–1824, https://doi.org/10.1007/978-3-319-48761-8_272
[39] F.-Z. Liu, J. Qin, Z. Li, C.-B. Yu, X. Zhu, H. Nagaumi, B. Zhang, Precipitation of dispersoids in Al–Mg–Si alloys with Cu addition, J. Mater. Res. Technol. 14 (2021) 3134–3139, https://doi.org/10.1016/j.jmrt.2021.08.123
[40] P. Jovičević-Klug, N. Lipovšek, M. Jovičević-Klug, B. Podgornik, Optimized preparation of deep cryogenic treated steel and Al-alloy samples for optimal microstructure imaging results, Mater. Today Commun. 27 (2021) 102211, https://doi.org/10.1016/J.MTCOMM.2021.102211
[41] M. Jovičević-Klug, P. Jovičević-Klug, T. Sever, D. Feizpour, B. Podgornik, Extraordinary nanocrystalline Pb whisker growth from Bi-Mg-Pb Pools in aluminum alloy 6026 moderated through oriented attachment, Page 1842, Nanomater 2021 11 (11) (2021) 1842, https://doi.org/10.3390/NANO11071842
[42] C. Niu, C. Li, Z. Du, C. Guo, Y. Jing, Thermodynamic assessment of the Bi-Mg binary system, Acta Metall. Sin. (Engl. Lett. 25 (2012) 19, https://doi.org/10.11890/1006-7191-121-19
[43] L. Wei, D. Wang, H. Li, D. Xie, F. Ye, R. Song, G. Zheng, S. Wu, Effects of Cryogenic treatment on the microstructure and residual stress of 7075 aluminum alloy, 273, Met 2018 8 (8) (2018) 273, https://doi.org/10.3390/MET8040273
[44] Q.C. Wang, L.T. Wang, W. Peng, Thermal stress relief in 7050 aluminum forgings by uphill quenching, Mater. Sci. Forum 490–491 (2005) 97–101, https://doi.org/10.4028/WWW.SCIENTIFIC.NET/MSF.490-491.97
[45] S. Pogatscher, H. Antrekowitsch, T. Ebner, P.J. Uggowitzer, The role of co-clusters in the artificial aging of AA6061 and AA6060, Light Met. 2012, Springer International Publishing, 2016, pp. 415–420, https://doi.org/10.1007/978-3-319-48179-1_70
[46] M. Werinos, H. Antrekowitsch, T. Ebner, R. Prillhofer, P.J. Uggowitzer, S. Pogatscher, Hardening of Al-Mg-Si alloys: effect of trace elements and prolonged natural aging, Mater. Des. 107 (2016) 257–268, https://doi.org/10.1016/j.matdes.2016.06.014
[47] K. Strobel, M.A. Easton, M.D.H. Lay, P.A. Rometsch, S. Zhu, L. Sweet, N.C. Parson, A.J. Hill, Quench sensitivity in a dispersoid-containing Al-Mg-Si alloy, Metall. Mater. Trans. A Phys. Metall. Mater. Sci. 50 (2019) 1957–1969, https://doi.org/10.1007/s11661-019-05130-2
[48] K. Buchanan, K. Colas, J. Ribis, A. Lopez, J. Garnier, Analysis of the metastable precipitates in peak-hardness aged Al-Mg-Si(-Cu) alloys with differing Si contents, Acta Mater. 132 (2017) 209–221, https://doi.org/10.1016/j.actamat.2017.04.037
[49] Y.X. Lai, B.C. Jiang, C.H. Liu, Z.K. Chen, C.L. Wu, J.H. Chen, Low-alloy-correlated reversal of the precipitation sequence in Al-Mg-Si alloys, J. Alloy. Compd. 701 (2017) 94–98, https://doi.org/10.1016/j.jallcom.2017.01.095
[50] Y.X. Lai, W. Fan, M.J. Yin, C.L. Wu, J.H. Chen, Structures and formation mechanisms of dislocation-induced precipitates in relation to the age-hardening responses of Al-Mg-Si alloys, J. Mater. Sci. Technol. 41 (2020) 127–138, https://doi.org/10.1016/j.jmst.2019.11.001
[51] A.K. Gupta, D.J. Lloyd, S.A. Court, Precipitation hardening in Al–Mg–Si alloys with and without excess Si, Mater. Sci. Eng. A 316 (2001) 11–17, https://doi.org/10.1016/S0921-5093(01)01247-3
[52] P.J. Bardziński, New Al3Si7 phase with tetragonal silicon structure in quasi-crystal-forming near-eutectic Al-Cu-Fe-Si alloys, J. Alloy. Compd. 869 (2021) 159349, https://doi.org/10.1016/j.jallcom.2021.159349
[53] M. Werinos, H. Antrekowitsch, E. Kozeschnik, T. Ebner, F. Moszner, J.F. Löffler, P.J. Uggowitzer, S. Pogatscher, Ultrafast artificial aging of Al-Mg-Si alloys, Scr. Mater. 112 (2016) 148–151, https://doi.org/10.1016/j.scriptamat.2015.09.037
[54] M.J. Starink, L.F. Cao, P.A. Rometsch, A model for the thermodynamics of and strengthening due to co-clusters in Al-Mg-Si-based alloys, Acta Mater. 60 (2012) 4194–4207, https://doi.org/10.1016/j.actamat.2012.04.032